Technical University of Denmark

DTU

Suppressed plastic deformation at blunt crack tips due to strain gradient effects

Mikkelsen, Lars Pilgaard; Goutianos, Stergios

DTU Library
Technical Information Center of Denmark

Suppressed plastic deformation at blunt crack tips due to strain gradient effects

Lars P. Mikkelsen[*] and Stergios Goutianos

Materials Research Division, Risø National Laboratory for Sustainable Energy,
Technical University of Denmark, DK-4000 Roskilde, Denmark

Abstract: Large deformation gradients occur near a crack-tip and strain gradient dependent crack-tip deformation and stress fields are expected. Nevertheless, for significant small length scales, a conventional elastic-plastic solution is obtained while for significant large length scales, a conventional elastic solution is obtained. This transition is investigated based on a finite strain version of the Fleck-Hutchinson strain gradient plasticity model from 2001. The predictions shows that for a large range of material parameters, the transition from the conventional elastic-plastic to the conventional elastic solution occurs for length scales going from 0.001 times the size of the reference size plastic zone to a length scale of the same order of magnitude.

Key words: blunt crack tip; strain gradient dependent plasticity; finite strain theory; finite elements.

1 Introduction

The deformation field near a crack-tip exhibits large plastic strain gradients (Fleck and Hutchinson, 1997) whereas an increasing number of experimental work reveals a size dependence of the plastic flow at the micron scale in the presence of strain gradients (Fleck et al., 1994; Poole, Ashby and Fleck, 1996; Stelmashenko et al., 1993; Stölken and Evans, 1998). Such a size dependency is absent in a conventional elastic-plastic theory. Therefore a plasticity theory which includes strain gradient effects will give more realistic predictions in the near crack tip region. Based on the Fleck and Hutchinson (1993) strain gradient plasticity theory which only includes rotation gradient dependency, Xia and Hutchinson (1996) found only a small effect on the stress field at a mode I loaded crack tip. On the other hand, still based on a small strain theory but including both stretch and rotation gradients in the phenomenological based strain gradient plasticity models (Fleck and Hutchinson, 1997; Fleck and Hutchinson, 2001) or in the mechanism-based based strain gradient plasticity models (Gao et al., 1999) a substantial increase in tractions ahead of the crack tip is observed (Chen and Wang, 2002; Chen et al., 1999;

---
[*] Corresponding author: E-mail: lapm@risoe.dtu.dk (L.P.Mikkelsen)

1

Komaragiri et al., 2008; Jiang et al., 2001).

From conventional plasticity studies, it is known that large deformation occurs in the blunting process of a crack tip (McMeeking, 1977) and that a small strain analysis has a tendency to underestimate the crack resistance during crack growth (Tvergaard and Hutchinson, 1992). On the other hand, based on a small strain theory, Wei and Hutchinson (1999) has shown a large effect of the strain gradient dependent term on the crack-growth behaviour. Only few studies based on a finite deformation version of a strain gradient dependent plasticity model have been performed, (Hwang et al., 2003).

Based on the finite strain version (Niordson and Redanz, 2004) of the strain gradient dependent plasticity model (Fleck and Hutchinson, 2001) a extensive parametric study of the crack tip field has been performed. The focus has been on the transition from predictions coinciding with the conventional elastic-plastic solution for suficiently small length scales to predictions coinciding with the conventional elastic solution for sufficiently large length scales. The size of the length scales should be correlated to a reference size of the plastic yielding zone and intermediate predictions are found for length scales in the region $\ell / R_p \in [0.001;1]$. For material length scales outside this region, either a conventional elastic-plastic simulation or a conventional elastic simulation are sufficient regarding both prediction of stationary crack-tip fields and crack-growth simulations.

2 Finite deformation strain gradient plasticity model

The material behaviour is modeled by a finite strain generalization (Niordson and Redanz, 2004) of the strain gradient plasticity theory of Fleck and Hutchinson (2001) in where an updated Langrangian formulation is adopted based on the work of (McMeeking and Rice, 1975; Yamada and Sasaki, 1995). In the following, only the brief description of the theory will be given. For more details see the paper by Niordson and Redanz (2004) together with its references to (Fleck and Hutchinson, 2001; Niordson and Hutchinson, 2003).

A standard power-law hardening material law is used with the hardening modulus h and the

tangent modulus E_t

$$\frac{1}{h} = \frac{1}{E_t} - \frac{1}{E} \quad ; \quad E_t = \frac{E}{n}\left(\frac{EE^p}{\sigma_y} + 1\right)^{\frac{1}{n}-1} \tag{1}$$

where E, σ_y and n denote the Youngs modulus, the initial yield stress and the hardening exponent of the material, respectivly. Different from a conventional plasticity theory, the tangent modulus E_t in (1) depends on the gradient dependent plastic strain E^p which is given by the incremental relation

$$\dot{E}^{p^2} = \dot{\varepsilon}^{p^2} + A_{ij}\dot{\varepsilon}^p_{,i}\dot{\varepsilon}^p_{,j} + B_{,i}\dot{\varepsilon}^p_{,i}\dot{\varepsilon}^p + C\dot{\varepsilon}^p \tag{2}$$

where the tensors A_{ij}, B_i, and C (Fleck and Hutchinson, 2001) depend on three length material length scales, ℓ_1, ℓ_2, ℓ_3, the outward normal to the plastic yield surface, $m_{ij} = 3S_{ij}/(2\sigma_{(e)})$, and their spatial derivatives, $m_{ij,k}$. The increment of the effective plastic strain is given by $\dot{\varepsilon}^p = \sqrt{3\dot{\varepsilon}^p_{ij}\dot{\varepsilon}^p_{ij}/2}$, the von Mises' stress by $\sigma_{(e)} = \sqrt{3S_{ij}S_{ij}/2}$ and the deviatoric stress by $S_{ij} = \sigma_{ij} - \delta_{ij}\sigma/3$ where σ_{ij} denotes the Cauchy stress tensor and δ_{ij} denotes Kronecker's delta. A standard tensor notation is adopted where latin indices range from 1 to 3 and repeated indices denote summation. The dotted terms denote incremental quantities and terms with $()_{,i}$ denote partial derivatives with respect to the coordinate x_i.

The equilibrium equation for the strain gradient plasticity model can be formulated through the virtual work in the current configuration (Fleck and Hutchinson, 2001):

$$\int_V (\sigma_{ij}\delta\dot{\varepsilon}_{ij} + (Q - \sigma_{(e)})\delta\dot{\varepsilon}^p + \tau_i\delta\dot{\varepsilon}^p_{,i})dV = \int_S (T_i\delta\dot{u}_i + t\delta\dot{\varepsilon}^p)dS \tag{3}$$

where ε_{ij} is the total strain. The term Q is defined as the work conjugate to the plastic strain ε^p which on incremental form is given by

$$\dot{Q} = \begin{cases} h\dot{\varepsilon}^p & , \text{ yielding} \\ \\ \dot{\sigma}_{(e)} & , \text{ elastic deformation} \end{cases} \tag{4}$$

The term $\tau_i \delta\varepsilon^p_{,i}$ in (3) represents the contribution due to the plastic strain gradients where τ_i are the higher order stresses.

3 Finite element formulation

Rewritting the virtual work (3) on an incremental form, see Niordson and Redanz (2004) including the plastic strain increment, $\dot{\varepsilon}^p$, as an additional fundamental unknown the finite element discretisation of the displacements and the plastic strain increments

$$\dot{u}_i = \sum_{n=1}^{k} N_i^n \dot{D}^n, \qquad \dot{\varepsilon}^p = \sum_{n=1}^{l} M^n \dot{\varepsilon}^p_n \tag{5}$$

leads to a equation system on the following form

$$\begin{bmatrix} \mathbf{K}_e & \mathbf{K}_{ep} \\ \mathbf{K}_{ep}^{\mathbf{T}} & \mathbf{K}_p \end{bmatrix} \begin{bmatrix} \dot{D} \\ \dot{\varepsilon}^p \end{bmatrix} = \begin{bmatrix} \dot{\mathbf{F}}_1 \\ \dot{\mathbf{F}}_2 \end{bmatrix} + \begin{bmatrix} \mathbf{C}_1 \\ \mathbf{C}_2 \end{bmatrix} \tag{6}$$

where expressions for all the terms in (6) can be found in Niordson and Redanz (2004). In (5), the N_i^n and M^n are the shape functions used for the displacement increment interpolation and the effective plastic strain increment interpolation, k and l are the number of nodes in the element used for the interpolations. The second term on the right-hand side of (6) represents the equilibrium correction factor, where $\mathbf{C}_1$ is the standard force equilibrium term (from where also the reaction forces can be extracted) and $\mathbf{C}_2$ is a non-standard equilibrium term related to the increments of the effective plastic strain. In the current simulations, only $\mathbf{C}_1$ is included in the

equilibrium correction term and $\mathbf{C_2} \equiv \mathbf{0}$.

A combined 8 and 4 noded element with $k = 8$ and $l = 4$ in (5) is used where N_i^n and M^n are given by standard isoparametric shape functions. The isoparametric geometric map from the local element coordinate system (ξ, η) to the global coordinate system (x_1, x_2) is based on the N_i^n shape function

$$x_i(\xi, \eta) = \sum_{n=1}^{k} N_i^n(\xi, \eta) x_i^n \qquad (7)$$

The element is integrated using 2x2 Gauss points. This combination was selected to avoid locking in the shear-dominated part near the crack tip and spurious zero energy modes in the effective plastic strain. For comparison, when both the displacements and effective plastic strain degrees of freedom were approximated by an 8-noded isoparametric element with 3x3 integration points significant locking in the effective plastic strain was found, see also Mikkelsen (2007).

From the incremental values the updated strains, ε_{ij}, stresses, σ_{ij}, higher order stress, τ_i and Q are found at each integration point. If an integration point is currently yielding, the effective plastic strain, E^p is updated. The yielding criterion for an integration point is $Q > Q_{max}$ where Q_{max} is the maximum value of Q obtained in the integration point with the initial value $Q_{max} = \sigma_y$. Elastic unloading of an integration point starts when $\dot{\varepsilon}^p < 0$. In the elastic region a sufficiently large hardening modulus, $h_{elastic} = 10^5 E$ is introduced to avoid spurious effective plastic strain increments. This corresponds to a internal elastic/elastic-plastic boundary condition $\dot{\varepsilon}^p = 0$ (Niordson, 2008). It has been found earlier by Mikkelsen (2007) that a converging solution is obtained for $h_{elastic} > 10^2 E$.

4 Crack-tip model

A semi-infinite crack is modelled in a homogeneous elastic-plastic solid under plane strain conditions. Due to symmetry only half the crack tip is modelled as depicted in Figure 1 where symmetry boundary conditions are applied along the symmetry line in front of the crack tip. In
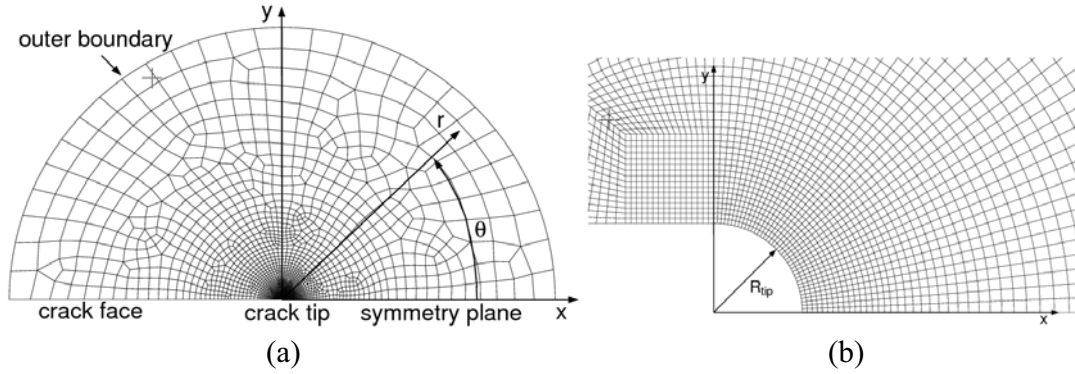
Figure 1 (a) Finite element mesh for the crack tip problem (b) Near-tip mesh for the mesh with the initial crack tip radius R_{tip}.

Figure 1, R_{tip} indicates the initial radius of the crack tip. The outer radius, R_{outer}, where the K_I-field is prescribed as the displacements in the x- and y-directions

$$\begin{Bmatrix} u_1 \\ u_2 \end{Bmatrix} = \frac{K_I}{2G}\sqrt{\frac{R_{outer}}{2\pi}} \begin{Bmatrix} cos(\theta/2)[\kappa-1+2sin^2(\theta/2)] \\ sin(\theta/2)[\kappa+1-2cos^2(\theta/2)] \end{Bmatrix} \qquad (8)$$

is chosen to be sufficiently large such that small scale yielding condition is satisfied. In equation (8), the angle θ is a measurement from the symmetry line in front of the crack tip, the term G denotes the shear modulus of the material and the term $\kappa = (3-4\nu)$ for the plane strain case. Except for a few cases, where $R_{outer} = 10^5 R_{tip}$, a outer radius of $R_{outer} = 10^3 R_{tip}$ is found to be sufficient in most of the finite element simulations giving a converged solution. In the context of the current strain gradient plasticity used (Fleck and Hutchinson, 2001) additional higher order boundary conditions need to be specified. Along all boundaries, no constraint is applied on $\dot{\varepsilon}^p$ corresponding to vanishing higher order stresses. This is do to the free surface along the crack face, the symmetry line in front of the crack tip and no plastic deformation near the outer boundary at $r = R_{outer}$.

The load level K_I will be represented in the study by a reference size of the plastic zone

$$R_p = \frac{1}{3\pi}\left(\frac{K_I}{\sigma_y}\right)^2 \qquad (9)$$

A dimensional study shows that the stress field in a given point in the initial blunted crack tip region here shown as the normal stress at the initial blunted crack tip will depend on the

following dimensionless terms

$$\frac{\sigma_{\theta\theta}^{tip}}{E} = f(\frac{\sigma_y}{E}, n, \nu, \frac{R_{tip}}{R_p}, \frac{\ell_1}{R_p}, \frac{\ell_2}{\ell_1}, \frac{\ell_3}{\ell_1}) \tag{10}$$

which make the basis for the parametric study. Later on, the predictions show that large incorporated material length scales result in finite element solutions coinciding with the purely elastic solution even though the material properties still include a yield stress and that it is the plastic strain gradients that are controlling the deformation stage. In order to compare the strain gradient dependent numerical predictions obtained in the following with classical elastic solutions, the analytical expressions are re-written using the reference size of the plastic zone, R_p as a measurement of the load level. The normal stress at the initial blunted crack tip $\sigma_{\theta\theta}^{tip} / \sigma_y$ (Creager and Paris, 1967) can based on a small strain elastic model be re-written as

$$\frac{\sigma_{\theta\theta}^{tip}}{E} = \frac{2K}{E\sqrt{\pi R_{tip}}}_I \quad \Rightarrow \quad \frac{\sigma_{\theta\theta}^{tip}}{\sigma_y} = \sqrt{12\frac{R_p}{R_{tip}}} \tag{11}$$

In addition, using the expression for the K_I stress field in front of the crack tip and compare the von Mises stress $\sigma_{(e)} = \sqrt{3s_{ij}s_{ij}/2}$ with the initial yield stress, σ_y, the actual size of the yielding size of the yielding region in the case of a large incorporated length scale can be estimated

$$\left.\begin{array}{l} \sigma_{\theta\theta} = \sigma_{rr} = K_I / \sqrt{2\pi r} \\ \sigma_{zz} = 2\nu K_I / \sqrt{2\pi r} \end{array}\right\} \quad \Rightarrow \quad \frac{R_{p(a)}}{R_p} = 0.24 \tag{12}$$

where $R_{p(a)}$ is measured from the surface of the blunted crack.

5 Numerical results

Figure 2 shows the near crack tip normalized stress field $\sigma_{\theta\theta} / \sigma_y$. The crack tip is loaded to a level where the reference size of the plastic zone is given by $R_p = 20R_{tip}$. Comparing the two contour plots in Figure 2 it can be seen that a large incorporated length scale results in a higher stress level in the region near the crack tip while the stress fields are approaching each other
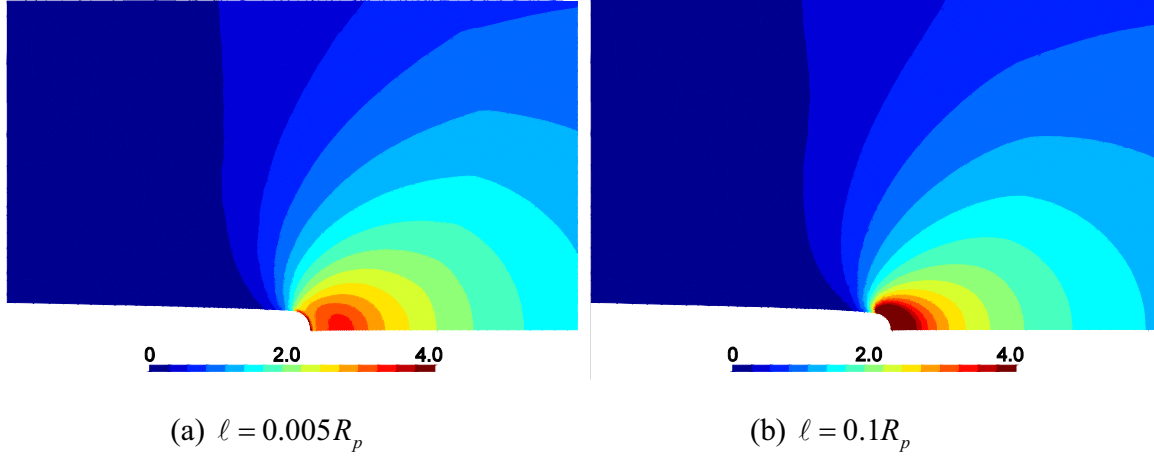
<center>(a) $\ell = 0.005R_p$ (b) $\ell = 0.1R_p$</center>

Figure 2 Stress field $\sigma_{\theta\theta}/\sigma_y$ at the crack tip for $\sigma_y/E = 0.01$; $\nu = 0.3$; $n = 5$ and the three length scales $\ell_1 = \ell_2 = \ell_3 = \ell$ loaded to $R_p/R_{tip} = 20$.

further away from the crack tip. The difference near the crack tip is due to the appearance of large plastic deformation gradients in the crack tip region, resulting in larger gradient dependent effective plastic strains, E^P, increasing the amount a plastic flow resistance and thereby lower the amount of plastic deformation in this region.

A crack tip loaded in mode I will in an isotropic homogeneous material results in crack growth along the symmetry line in front of the crack tip. Figure 2 shows the normalized stress, $\sigma_{\theta\theta}/\sigma_y$, along this path for a fixed $R_p/R_{tip} = 20$ ratio and with material parameters given by $\sigma_y/E = 0.01$; $\nu = 0.3$; $n = 5$ with the three length scales $\ell_1 = \ell_2 = \ell_3 = \ell$. The two cases from Figure 2 are included in Figure 3. Along the x-axis, the normalized distance from the crack-tip in the deformed configuration is shown. For sufficiently small incorporated length scales, $\ell < 0.0025R_p$, the strain gradient dependent terms does not influence the simulations. Therefore, the predictions are given by a conventional elastic-plastic solution. On the other hand, for sufficiently large material length scales, $\ell > 0.25R_p$, the strain gradient dependent terms will dominate the solution preventing essentially any plastic deformation to develop. Therefore, the solution will for these large lengths scales coincide with the conventional elastic solution. Only in the intermediate region, $0.0025 < \ell/R_p < 0.25$, an advanced gradient dependent plasticity model
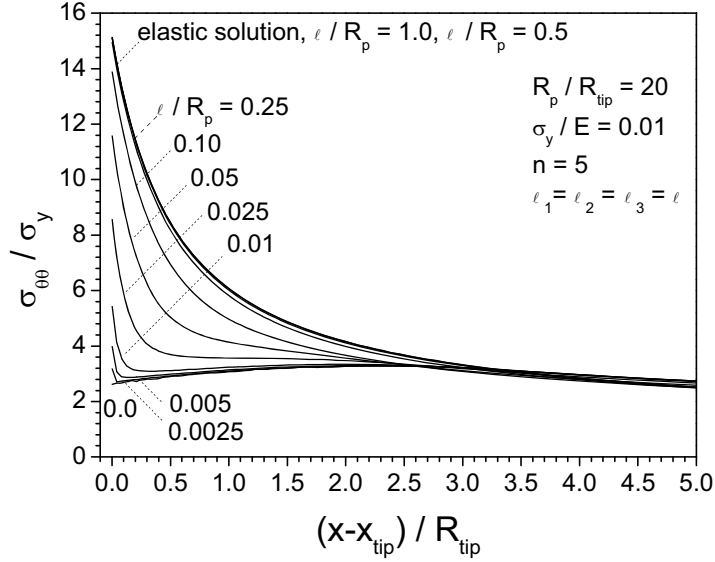
<center>8</center>

Figure 3 The stress field, $\sigma_{\theta\theta}$, along the symmetry line in front of the crack tip.

is needed, predicting a significant dependency on the actually value of the incorporated length scale.

Due to the finite radius of the initial crack tip, the stress value at the crack tip will have a finite value, $\sigma_{\theta\theta}^{tip}$. For large incorporated length scales the solution only differ 2% from the small strain elastic prediction $\sigma_{\theta\theta}^{tip} / \sigma_y = 15.5$ from equation (11). Using the finite crack tip stress $\sigma_{\theta\theta}^{tip}$ to represent the stress field in front of the crack tip, a detailed parameter study is possible.

In Figures 4-6, a parametric study with the offset from the material properties

$$\sigma_y / E = 0.01 \; ; \; \nu = 0.3 \; ; \; n = 5 \; ; \; \ell_1 = \ell_2 = \ell_3 = \ell \tag{13}$$

are investigated regarding the dependency of the crack tip stress on the parameters

$$R_p / R_{tip} \; ; \; n \; ; \; \sigma_y / E \; ; \; \ell / R_p \tag{14}$$

The study focuses on the transition from a conventional elastic-plastic solution for sufficiently
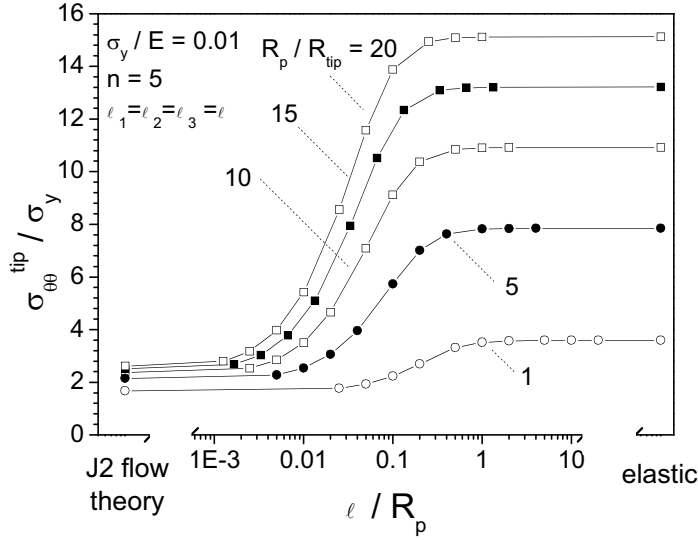
9

Figure 4 The stresses at the blunted crack tip, $\sigma_{\theta\theta}^{tip}/\sigma_y$, for different load levels.

small length scales to the elastic solution for sufficiently large length scale. By normalizing the length scale with the reference size of the plastic zone, a rather similar transition region is obtained for all the investigated R_p/R_{tip} ratios.

Figure 4 shows the dependency of the ratio between the reference of the plastic zone and the initial radius of the crack tip, R_p/R_{tip}, on the crack tip stress, $\sigma_{\theta\theta}^{tip}/\sigma_y$. From Figure 4, it can be seen that for all the load levels studied for the default case shown in (13), the transition from the conventional elastic-plastic solution to the conventional elastic solution occurs for length scale in the range $\ell/R_p \in [10^{-3};1]$. For length scale $\ell/R_p < 0.001$ the predictions coincide with a solution based on a conventional J_2- flow theory while a purely elastic prediction is obtained for $\ell/R_p > 1$. Even for much larger load levels approaching the case of a sharp crack, see later, the transition is found in nearly the same length scale range switching slightly towards a little smaller length scales for higher R_p/R_{tip} ratios.

The dependency on the strain hardening exponent, n, is shown in Figure 5. The stress level at the
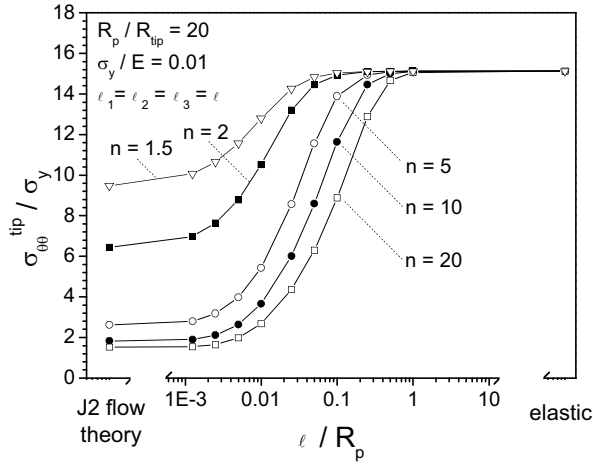
Figure 5 The stresses at the blunted crack tip, $\sigma_{\theta\theta}^{tip}/\sigma_y$, for different strain hardening exponents n.

crack-tip is found strongly to depend on the hardening exponent for small length scales in agreement with the corresponding dependency predicted by conventional plasticity theories, see e.g. McMeeking (1977). For large incorporated length scales, the predictions approach the elastic solution, a solution which is independent on the hardening exponent. For intermediate length scales, $\ell/R_p \in [10^{-3}; 1]$, a smooth transition is found for all hardening exponents.
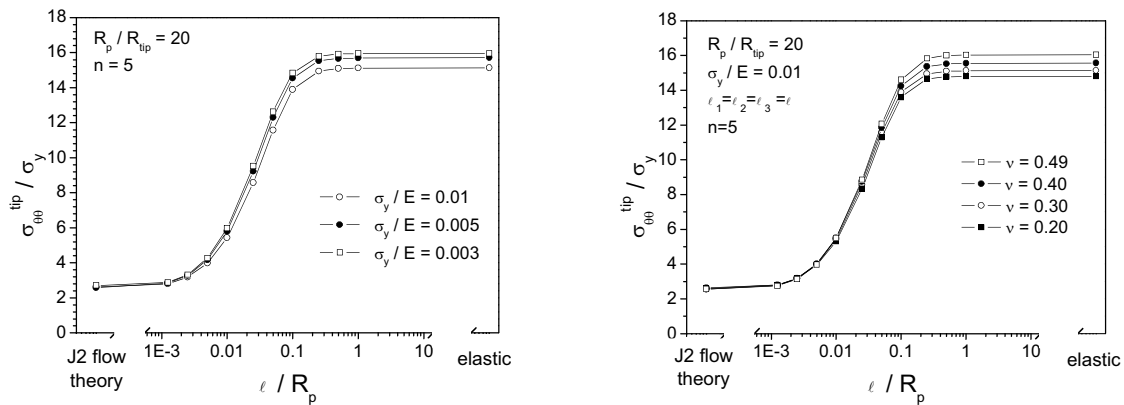

Figure 6 The stresses at the blunted crack tip, $\sigma_{\theta\theta}^{tip}/\sigma_y$, for (a) different yield stresses (b) different Poisson's ratios ν.

Figure 6 shows the dependency of the initial yield stress, σ_y / E , and Poisson's ratio, ν on the normalized normal stress $\sigma_{\theta\theta}^{tip} / \sigma_y$ at the crack tip. Even though the dependency is found to be small for both cases, it is more pronounced for large incorporated length scale corresponding to the conventional elastic solution. Nevertheless, this dependency of the elastic solution is purely due to large strain effects. A small strain elastic simulation of the normalized stress variation $\sigma_{\theta\theta} / \sigma_y$ around the crack tip results in coinciding solutions for different yield stresses and Poisson's ratios. Regarding the Poisson's ratios, this is in agreement with the fact that the linear elastic crack tip solution is independent of the elastic constitutive properties as all boundary conditions in principle can be given by prescribed stresses, see Michell (1899). On the other hand, for small incorporated length scales and thereby with dominating plastic deformations the material will behave as a material with an effective Poisson's ratio approaching ½ for all cases and no dependency on the elastic Poisson's ratio will be expected. For a fixed ratio R_p / R_{tip} , a change in the yield stress corresponds to a different load level, K_I , corresponding to (9). Nevertheless, due to the normalization of the stresses at the crack-tip, $\sigma_{\theta\theta}^{tip} / \sigma_y$, the solutions are found to nearly coincide for small incorporated material length scales ℓ .

Based on (Fleck and Hutchinson (1997) strain gradient dependent plasticity model in a small strain version, Chen et al. (1999) predicted in a sharp crack tip analysis for $\ell / R_p = 0.1$, a large dependency of the stress field in the near crack tip field, $x - x_{tip} < 0.3\ell$ when the Poisson's ratio approaching 0.5. From the latter Figure 12 and Figure 13, it can be seen that this corresponds to a case where the stress field is approximately given by the elastic solution. The dependency in the present solution for a blunted crack based on a finite strain analysis does not show this strong dependency.

Even though the stress field coincides with the conventional elastic solution for sufficiently large length scale it does not mean that the material is not yielding. Actually, the gradient dependent term is only active in the presence of plastic strain gradients. On the other hand, for sufficiently large material length scales, all significant plastic deformations at the crack-tip are suppressed by the gradient dependent term resulting essentially in a linear elastic behavior. The yielding region
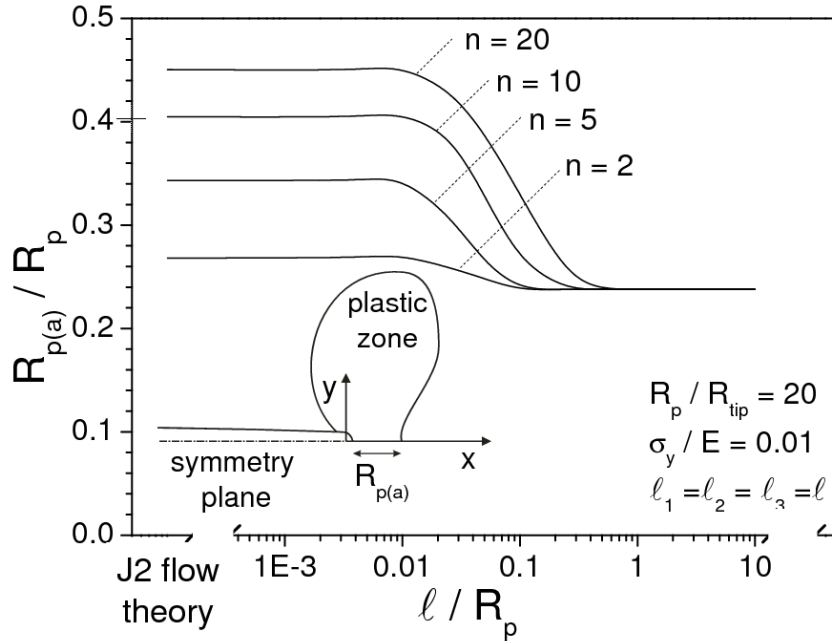
Figure 7 The actual size of the yielding zone found for different hardenings exponents.

will in this "elastic" case have a size coinciding with the estimate $R_{p(a)} / R_p = 0.24$, see equation (12).

Figure 7 shows the size of the yielding region measured from the crack tip to the end of the yielding zone along the center-line in front of the crack tip. This distance is normalized with the calculated reference size of the yielding region R_p. For small incorporated length scales Figure 7 shows a large dependency of the size of the yielding zone on the hardening exponent. A dependency which, similar to Figure 5, vanishes for large incorporated length scales. For large length scales, the size is found to coincide with the elastic K_I-field estimation, $R_{p(a)} / R_p = 0.24$.

In all the previous figures, the three length scales where chosen to be equal to each other $\ell_1 = \ell_2 = \ell_3 = \ell$ even though this will rarely be the case in a real material. Figure 8 compares the case $\ell_1 = \ell_2 = \ell_3 = \ell$ with cases where only one of the three length scale is non-vanishing. In Figure 8 it can be seen that for a given length scale, ℓ, $\ell_2 = \ell$ and $\ell_3 = \ell$ gives the smallest effects, while $\ell_1 = \ell$ gives the largest strain gradient effects. Actually the case $\ell_1 = \ell$ is seen to
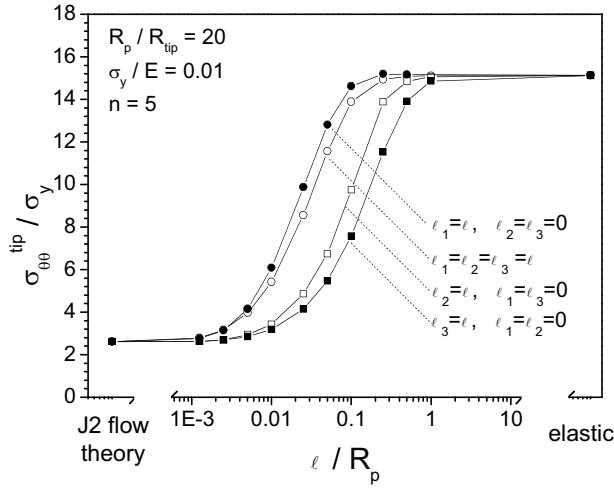
Figure 8 The stresses at the blunted crack tip, $\sigma_{\theta\theta}^{tip}/\sigma_y$, for materials with different combinations of length scales

results in a larger effects than $\ell_1 = \ell_2 = \ell_3 = \ell$ indicating that the length scales ℓ_2 and ℓ_3 have

a reducing effect on ℓ_1 with respect to the size of the stress level at the crack tip, $\sigma_{\theta\theta}^{tip}$.
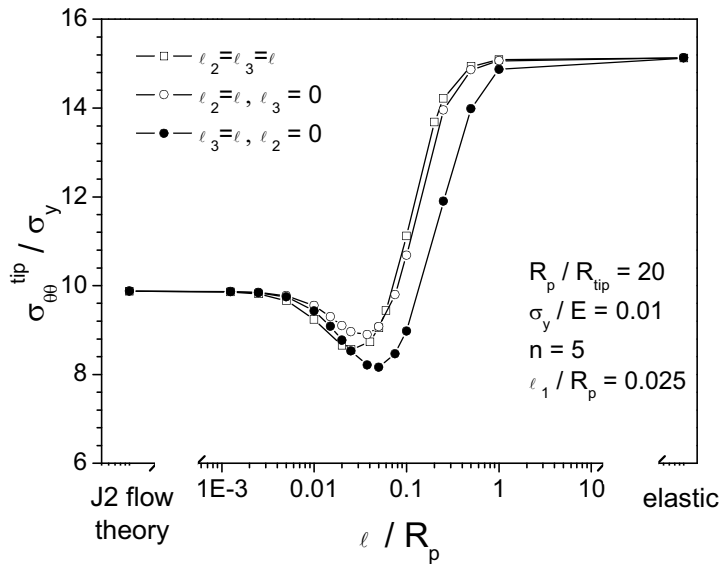

Figure 9 The stresses at the blunted crack tip, $\sigma_{\theta\theta}^{tip}/\sigma_y$, for materials with a fixed length scale $\ell_1/R_p = 0.025$.
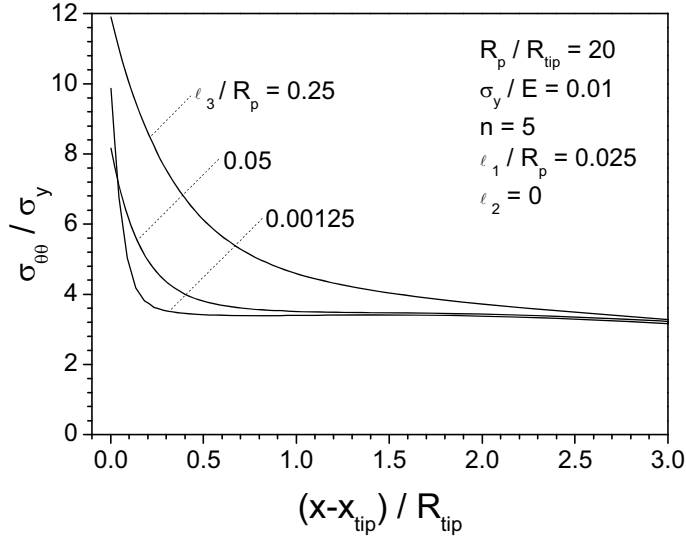
Figure 10 The stresses variation, $\sigma_{\theta\theta} / \sigma_y$, in front of the blunted crack tip.

The reducing effect of ℓ_2 and ℓ_3 is studied in Figure 9 where the length scale $\ell_1 = 0.025 R_p$ is kept constant while the other two length scales are varied. From Figure 9 it can be seen that it is the length scale ℓ_3 which has the largest reducing effect on the length scale ℓ_1. Fleck and Hutchinson (2001) noted that the effects of the length scales ℓ_2 and ℓ_3 disappear for vanishing rotational gradients while the contribution from ℓ_1 comes both from stretching and rotational gradients. Therefore, the shear deformation at the crack-tip will introduce additional strain hardening due to the occurrence of the length scales ℓ_2 and ℓ_3 which will redistribute the stress field. These effect can be seen in Figure 10; A increasing size of the length scale ℓ_3 increases the overall normal stress level, $\sigma_{\theta\theta}$, even though the peak stress at the crack tip is getting lower for some intermediate value of the third length scale ℓ_3.

Figure 11 shows the conventional elastic and elastic-plastic stress variation in front of an initial blunted crack tip as a function on the ratio between the reference size of the plastic zone, R_p, and the initial radius of the crack-tip, R_{tip}. For a significant large R_p / R_{tip} ratio, the solution
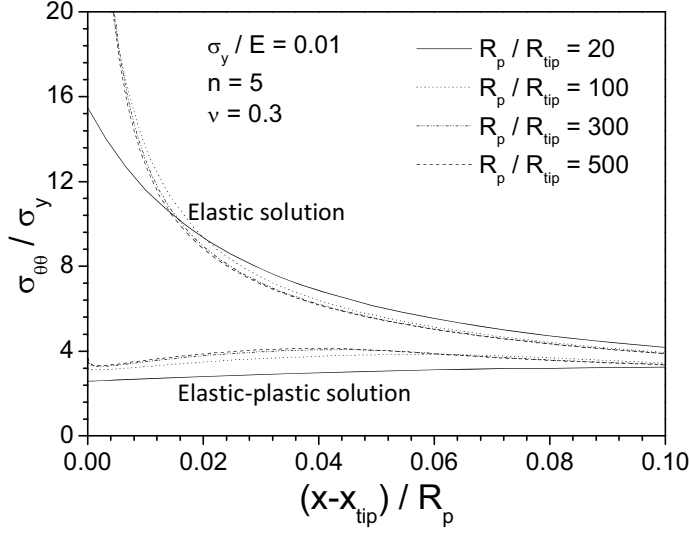
Figure 11 The conventional elastic and elastic-plastic stresses variation, $\sigma_{\theta\theta}/\sigma_y$, in front of the blunted crack tip approaching a sharp crack tip.

converges to the solution given for a sharp crack tip in agreement with McMeeking (1977). Except for the large strain contribution, the converged elastic solution is simply given by K_I stress field $\sigma_{\theta\theta}/\sigma_y = \sqrt{2R_p/3x}$. The solution $R_p/R_{tip} = 20$ corresponds to the solution shown earlier in Figure 3 and for $R_p/R_{tip} > 300$ the solution is found to converge to the sharp crack-tip solution.

In the case of an initially sharp crack tip, Figure 12 shows the length scale dependent solution for the default case from equation (13). For this specific case, a transition from the conventional elastic-plastic solution for $\ell/R_p < 0.001$ to the elastic solution for $\ell/R_p > 0.5$ is observed. Similar to the predictions for the initial blunted crack-tips, it is only necessary to base the finite element simulation on an enhanced strain gradient dependent plasticity model for intermediate length scales, specified by the range $\ell/R_p \in [10^{-3};1]$. For smaller length scales a conventional elastic-plastic material model is sufficient, while the strain gradient dependent terms are
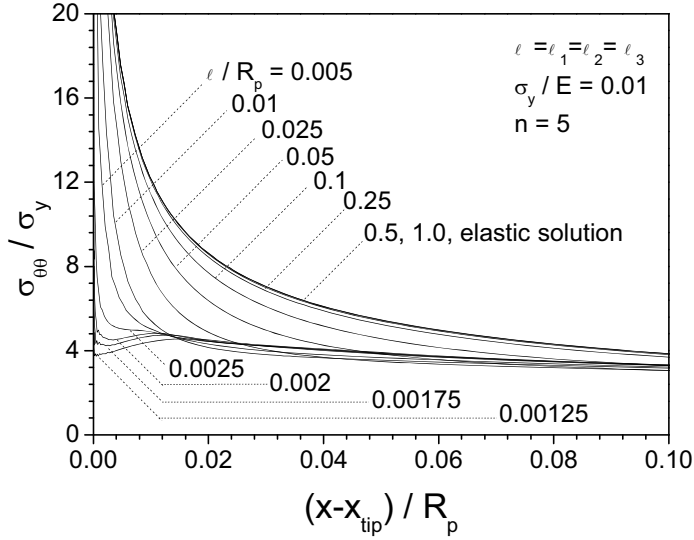
16

Figure 12 The stresses variation, $\sigma_{\theta\theta}/\sigma_y$, in front of an initial sharp crack tip.

dominant for larger length scale in such a way that all plastic deformation is essentially suppressed and predictions based on an elastic model are significant.

Figure 13 shows the converged blunted shape of an initially sharp crack as a function of the normalized incorporated length scale ℓ/R_p. A similar transition to Figure 12 is observed in Figure 13 going from a conventional elastic-plastic solution for vanishing length scale to a elastic solution for significant large length scale $\ell > 0.5R_p$. Experimental measurement of the shape of the blunted crack tip could be a way to identify the influence of gradient dependent terms at a specific deformed crack-tip. Shih (1981) defined a measurement of the crack tip opening as the opening δ_t in an angle $45°$ behind the crack tip as indicated by the dotted line in Figure 13. For the specific default case, equation (13), the crack opening measurement (defined as the double of the one shown figure 13) is found to vary from the conventional elastic-plastic solution $\delta_t = 0.025$ for $\ell/R_p < 0.001$ to the conventional elastic solution $\delta_t = 0.0036$ for $\ell/R_p > 0.5$.
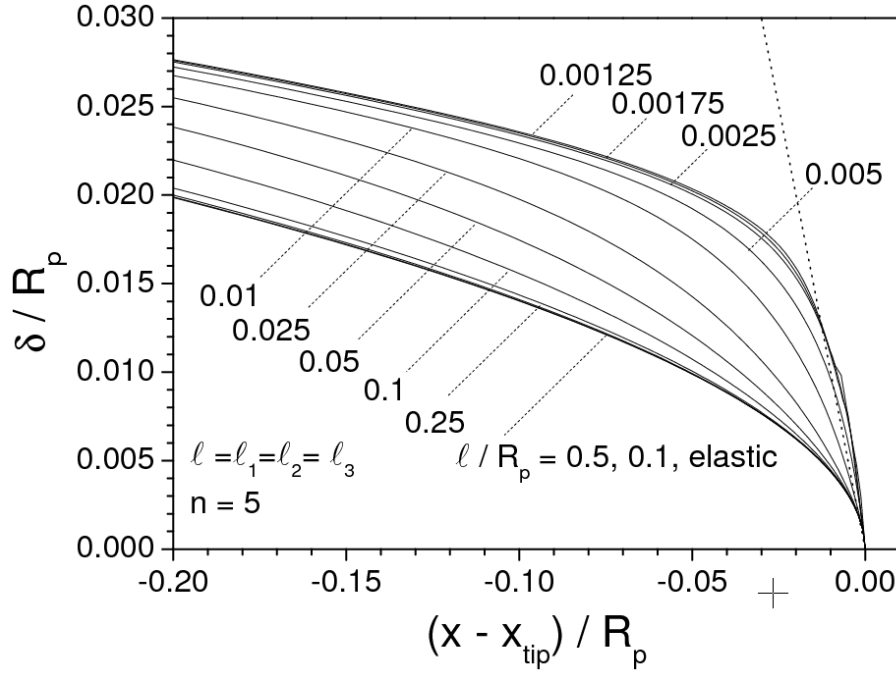
Figure 13 The shape of the blunting of an initially sharp crack tip.

6 Discussion

Based on the normalized stress-level at the crack tip, $\sigma_{\theta\theta}^{tip} / \sigma_y$, of an initially blunted crack a thorough parametric study has been performed investigating the strain gradient dependent suppression of the plastic deformation at an initially blunted crack-tip in a homogeneous elastic-plastic power-law hardening isotropic material. The study shows that for all material parameters studied a transition from predictions coinciding the conventional elastic-plastic solution for $\ell < 0.001R_p$ to predictions coinciding the conventional elastic solution for $\ell > R_p$ is obtained. In the intermediate region $0.001R_p < \ell < R_p$, a smooth transition occurs. These results can be used judging whether a conventional elastic-plastic model, the more complex strain gradient dependent elastic-plastic model or a simple linear elastic model are required predicting crack-tip properties. Therefore, based on a conventional crack-tip or crack growth problem, the size of the yielding region should be considered. If the size is larger than 1000 times the material length scale, a conventional plasticity theory is sufficiently. On the other hand, if the size of the yielding region is less than the material length scale, essentially all plastic deformation will be suppressed and a conventional elastic prediction are sufficient. On the other hand, if the size is in the intermediate

18

range, a full strain gradient dependent plasticity simulation is necessary.

Reference

Chen, J.Y., Wei, Y., Huang, Y., Hutchinson, J.W., Hwang, K.C., 1999. The crack tip fields in strain gradient plasticity: the asymptotic and numerical analyses. Eng. Fract. Mech. 64 (5) 625-648.

Chen, S.H., Wang, T.C., 2002. Finite element solutions for plane strain mode I crack with strain gradient effects. Int. J. Solids Struct. 39 (5) 1241-1257.

Creager, M., Paris, P.C., 1967. Elastic field equations for blunt cracks with reference to stress corrosion cracking. Int. J. Fract. Mech. 3 247-252.

Fleck, N.A., Hutchinson, J.W., 2001. A reformulation of strain gradient plasticity. J. Mech. Phys. Solids 49 (10) 2245-2271.

Fleck, N.A. and Hutchinson, J.W., 1997. Strain Gradient Plasticity. Adv. in Appl. Mech. 33 295-361

Fleck, N.A., Hutchinson, J.W., 1993. A phenomenological theory for strain gradient effects in plasticity. J. Mech. Phys. Solids 41 (12) 1825-1857.

Fleck, N.A., Muller, G.M., Ashby, M.F., Hutchinson, J.W., 1994. Strain gradient plasticity: Theory and experiment. Acta Metallurgica et Materialia, 42 (2) 475-487.

Gao, H., Huang, Y., Nix, W.D., Hutchinson, J.W., 1999. Mechanism-based strain gradient plasticity— I. Theory. Journal of the Mechanics and Physics of Solids, 47 (6) 1239-1263.

Hwang, K.C., Jiang, H., Huang, Y., Gao, H., 2003. Finite deformation analysis of mechanism-based strain gradient plasticity: torsion and crack tip field. Int. J. Plast. 19 (2) 235-251.

Jiang, H., Huang, Y., Zhuang, Z., Hwang, K.C., 2001. Fracture in mechanism-based strain gradient plasticity. J. Mech. Phys. Solids 49 (5) 979-993.

Komaragiri, U., Agnew, S.R., Gangloff, R.P., Begley, M.R., 2008. The role of macroscopic hardening and individual length-scales on crack tip stress elevation from phenomenological strain gradient plasticity. J. Mech. Phys. Solids 56 (12) 3527-3540.

McMeeking, R.M., 1977. Finite deformation analysis of crack-tip opening in elastic-plastic materials and implications for fracture. J. Mech. Phys. Solids 25 (5) 357-381.

McMeeking, R.M., Rice, J.R., 1975. Finite-element formulations for problems of large elastic-plastic deformation. Int. J. Solids Struct. 11 (5) 601-616.

Michell, J.H., 1899. On the direct determination of stress in an elastic solid, with application to the theory of plates. Proc. the London Mathematical Society XXXI 100-124.

Mikkelsen, L.P., 2007. Implementing a gradient dependent plasticity model in ABAQUS. SIMULIA, Paris, France, pp. 482-492.

Niordson, C.F., 2008. On higher-order boundary conditions at elastic–plastic boundaries in strain-gradient plasticity. Philosophical Magazine 88 (30) 3731-3745.

Niordson, C.F., Hutchinson, J.W., 2003. Non-uniform plastic deformation of micron scale objects. Int. J. Num. Meth. Eng. 56 (7) 961-975.

Niordson, C.F., Redanz, P., 2004. Size-effects in plane strain sheet-necking. J. Mech. Phys.

Solids 52 (11) 2431-2454.

Poole, W.J., Ashby, M.F., Fleck, N.A., 1996. Micro-hardness of annealed and work-hardened copper polycrystals. Scripta Materialia 34 (4) 559-564.

Shih, C.F., 1981. Relationships between the J-integral and the crack opening displacement for stationary and extending cracks. J. Mech. Phys. Solids 29 (4) 305-326.

Stelmashenko, N.A., Walls, M.G., Brown, L.M., Milman, Y.V., 1993. Microindentations on W and Mo oriented single crystals: An STM study. Acta Metallurgica et Materialia 41 (10) 2855-2865.

Stölken, J.S., Evans, A.G., 1998. A microbend test method for measuring the plasticity length scale. Acta Materialia, 46 (14) 5109-5115.

Tvergaard, V., Hutchinson, J.W., 1992. The relation between crack growth resistance and fracture process parameters in elastic-plastic solids. J. Mech. Phys. Solids 40 (6) 1377-1397.

Wei, Y., Hutchinson, J.W., 1999. Models of interface separation accompanied by plastic dissipation at multiple scales. Int. J. Fract. Mech. 95 1-17.

Xia, Z.C., Hutchinson, J.W., 1996. Crack tip fields in strain gradient plasticity. J. Mech. Phys. Solids 44 (10) 1621-1648.

Yamada, Y., Sasaki, M., 1995. Elastic-plastic large deformation analysis program and lamina compression test. Int. J. Mech. Science 37 (7) 691-707.